Subwavelength imaging in photonic crystals

Chiyan Luo,* Steven G. Johnson, and J. D. Joannopoulos

Department of Physics and Center for Materials Science and Engineering, Massachusetts Institute of Technology, Cambridge, Massachusetts 02139, USA

J. B. Pendry

Condensed Matter Theory Group, The Blackett Laboratory, Imperial College, London SW7 2BZ, United Kingdom

We investigate the transmission of evanescent waves through a slab of photonic crystal and explore the recently suggested possibility of focusing light with subwavelength resolution. The amplification of near-field waves is shown to rely on resonant coupling mechanisms to surface photon bound states, and the negative refractive index is only one way of realizing this effect. It is found that the periodicity of the photonic crystal imposes an upper cutoff to the transverse wave vector of evanescent waves that can be amplified, and thus a photonic-crystal superlens is free of divergences even in the lossless case. A detailed numerical study of the optical image of such a superlens in two dimensions reveals a subtle and very important interplay between propagating waves and evanescent waves on the final image formation. Particular features that arise due to the presence of near-field light are discussed.

I. INTRODUCTION

Negative refraction of electromagnetic waves, initially proposed in the 1960s,[1] recently attracted strong research interest[2–16] and generated some heated debate.[17–29] In particular, much attention was focused on the intriguing possibility of *superlensing* suggested in Ref. 5: a slab of uniform "left-handed material" with permittivity $\epsilon = -1$ and permeability $\mu = -1$ is capable of capturing both the propagating and evanescent waves emitted by a point source placed in front of the slab and refocusing them into a *perfect* point image behind the slab. While the focusing effect of propagating waves can be appreciated from a familiar picture of rays in geometric optics, it is amazing that perfect recovery of evanescent waves may also be achieved via *amplified* transmission through the negative-index slab. Some of the discussion of this effect relies on an effective-medium model[6] that assigns a negative ϵ and a negative μ to a periodic array of *positive*-index materials: i.e., a photonic crystal.[30] Such an effective-medium model holds for large-scale phenomena involving propagating waves, provided that the lattice constant a is only a small fraction of the free-space wavelength in the frequency range of operation. However, in the phenomenon of superlensing, in which the subwavelength features themselves are of central interest, an effective-medium model places severe constraints on the lattice constant a: it must be smaller than the subwavelength details we are seeking to resolve. The question of whether and to what extent superlensing would occur in the more general case of photonic crystals still remains unclear.

Recently, we showed that all-angle negative refraction (AANR) is possible using a photonic crystal with a positive index, and we demonstrated imaging with a resolution below or on the order of wavelength in this approach.[12,15] In this paper, we investigate the possibility of photonic-crystal superlensing in detail by studying the transmission of evanescent waves through a slab of such a photonic crystal. It is important to note that the transmission considered here differs fundamentally from its conventional implication of energy transport, since evanescent waves need not carry energy in their decaying directions. Thus, it is possible to obtain transmission amplitudes for evanescent waves greatly exceeding unity without violating energy conservation. Here, we discuss two mechanisms linking amplification of evanescent waves to the existence of bound slab photon states. These bound states are decoupled from the continuum of propagating waves, thus our findings are distinct from the effect of Fano resonances[31] in electromagnetism, which were recently studied in the context of patterned periodic structures[32–36] and surface-plasmon-assisted energy transmission.[37–39] As for the problem of negative refraction, we have found that the concept of superlensing does *not* in general require a negative refractive index. Moreover, we argue that the surface Brillouin zones of both photonic crystals and periodic effective media provide a natural upper cutoff to the transverse wave vector of evanescent waves that can be amplified, and thus no divergences exist at large transverse wave vectors[24] in photonic crystals or in effective media.[27] As with effective media, the lattice constant of photonic crystals must always be smaller than the details to be imaged. We derive the ultimate limit of superlens resolution in terms of the photonic-crystal surface periodicity and infer that resolution arbitrarily smaller than the wavelength should be possible in principle, provided that sufficiently high dielectric contrast can be obtained. We pursue these ideas in realistic situations by calculating the bound photon states in carefully designed two-dimensional (2D) and 3D slabs of AANR photonic crystals and present a comprehensive numerical study of a 2D superlensing structure. A subtle and very important interplay between propagating waves and evanescent waves on image formation is revealed, which makes the appearance of the image of a superlens substantially different from that of a real image behind a conventional lens. These numerical results confirm the qualitative
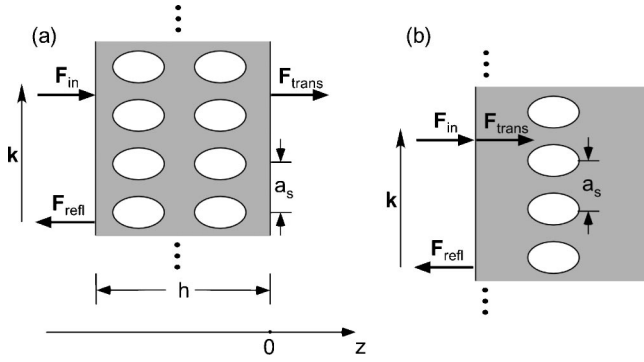
FIG. 1. Illustration of light-wave transmission through a photonic crystal. (a) Transmission through a slab of photonic crystal. The incident field $\mathbf{F}_{in}$ and the reflected field $\mathbf{F}_{refl}$ are measured at the left surface of the slab ($z=-h$), and the transmitted field $\mathbf{F}_{trans}$ is measured at the right surface of the slab ($z=0$). (b) Transmission through a boundary surface between air and a semi-infinite photonic crystal. The incident field $\mathbf{F}_{in}$, the reflected field $\mathbf{F}_{refl}$, and the transmitted field $\mathbf{F}_{trans}$ are all measured at the air/photonic-crystal interface. In both figures, $\mathbf{k}$ is the transverse wave vector of light and a_s indicates the surface periodicity.

discussions in this paper and can be readily compared to experimental data.

This paper is organized as follows. Section II is a general discussion for amplified transmission of evanescent waves through a photonic-crystal slab. Section III considers the implementation of superlensing in photonic crystals and its ultimate resolution limit and, also, describes qualitatively the expected appearance of the image of a superlens. Section IV presents numerical results for superlensing in a model photonic crystal. Section V discusses further aspects of superlensing in photonic crystals, and Sec. VI summarizes the paper.

II. ORIGIN OF NEAR-FIELD AMPLIFICATION

Let us first consider the transmission of a light wave through a slab of lossless dielectric structure [Fig. 1(a)], periodic in the transverse direction, at a definite frequency ω (with free-space wavelength $\lambda = 2\pi c/\omega$) and a definite transverse wave vector $\mathbf{k}$. Let the slab occupy the spatial region $-h < z < 0$, and in this paper we also assume a mirror symmetry with respect to the plane $z=-h/2$ at the center of the dielectric structure. The transmission through a finite-slab structure can be conceptually obtained by first considering the transmission through a single interface between air and the photonic crystal [Fig. 1(b)] and then summing up all the contributions as light bounces back and forth inside the slab. The incident field $\mathbf{F}_{in}$, the reflected field $\mathbf{F}_{refl}$, and the transmitted field $\mathbf{F}_{trans}$ are related to each other by the transmission coefficient t, defined formally by $\mathbf{F}_{trans} = t\mathbf{F}_{in}$, and the reflection coefficient r, defined formally by $\mathbf{F}_{refl} = r\mathbf{F}_{in}$. Here, all fields are understood to be column vectors expressed in the basis of all the eigenmodes of the corresponding medium, with transverse wave vectors differing from $\mathbf{k}$ only by a reciprocal lattice vector of the surface. In this way, t and r are matrices represented in these basis modes. The overall transmission coefficient through the slab structure can be written as

$$t = t_{p\text{-}a}(1 - T_{\mathbf{k},p}r_{p\text{-}a}T_{\mathbf{k},p}r_{p\text{-}a})^{-1}T_{\mathbf{k},p}t_{a\text{-}p}. \tag{1}$$

In Eq. (1), $t_{a\text{-}p}$ and $t_{p\text{-}a}$ are the transmission coefficients through the individual interfaces from air to the photonic crystal and from the photonic crystal to air, respectively, $r_{p\text{-}a}$ is the reflection coefficient on the photonic-crystal/air boundary, and $T_{\mathbf{k},p}$ is the translation matrix that takes the fields from $z=-h$ to $z=0$ inside the photonic crystal. When h is an integral multiple of the crystal's z period, $T_{\mathbf{k},p}$ is diagonal with elements $e^{ik_z h}$ for a crystal eigenmode of Bloch wave vector $\mathbf{k}+k_z\hat{\mathbf{z}}$, with $\mathrm{Im}\,k_z \geq 0$. In what follows, we discuss the possibility of amplification in t, beginning with the diagonal element that describes the zeroth-order transmission— i.e., transmission of waves with $\mathbf{k}$ in the first surface Brillouin zone, referred to as t_{00}.

Generally speaking, Eq. (1) describes a transmitted wave that is exponentially small for large enough $|\mathbf{k}|$. This can be seen in the special case of a slab of uniform material with permittivity ϵ and permeability μ, where all the matrices in Eq. (1) can be expressed in the basis of a single plane wave and thus reduce to a number. In particular, $T_{\mathbf{k},p} = \exp(ik_z h) = \exp(ih\sqrt{\epsilon\mu\omega^2/c^2 - |\mathbf{k}|^2})$, which becomes exponentially small as $|\mathbf{k}|$ goes above $\sqrt{\epsilon\mu}\,\omega/c$. Equation (1) then becomes a familiar elementary expression

$$t_{00} = \frac{t_{p\text{-}a}t_{a\text{-}p}e^{ik_z h}}{1 - r_{p\text{-}a}^2 e^{2ik_z h}}. \tag{2}$$

Equation (2) has an exponentially decaying numerator, while for fixed $r_{p\text{-}a}$ the denominator approaches 1. Thus, waves with large enough $|\mathbf{k}|$ usually decay during transmission in accordance with their evanescent nature.

There exist, however, two separate mechanisms by which the evanescent waves can be greatly amplified through transmission, a rather unconventional phenomenon. The first mechanism, as proposed in Ref. 5, is based on the fact that under appropriate conditions, the reflection and transmission coefficients through individual interfaces can become *divergent* and may thus be called a *single-interface resonance*. For example, under the condition of single-interface resonance, $t_{a\text{-}p}, t_{p\text{-}a}, r_{p\text{-}a} \rightarrow \infty$, and in the denominator of Eq. (2) the term $r_{p\text{-}a}^2\exp(2ik_z h)$ dominates over 1. In this limit, Eq. (2) becomes

$$t_{00} = \frac{t_{p\text{-}a}t_{a\text{-}p}}{-r_{p\text{-}a}^2}e^{-ik_z h}. \tag{3}$$

The divergences in Eq. (3) cancel each other, and the net result is that for large $|\mathbf{k}|$, $t_{00} = \exp(-ik_z h)$, leading to amplification of exactly the right degree to focus an image. The same arguments can be applied to the general case of Eq. (1), as long as k_z is regarded as the z component of the corresponding eigenmode's wave vector with the *smallest* imaginary part ($\mathrm{Im}\,k_z$), which produces the dominant term via $e^{ik_z h}$. As elements of $r_{p\text{-}a}$ grow sufficiently large, the matrix product $T_{\mathbf{k},p}r_{p\text{-}a}T_{\mathbf{k},p}r_{p\text{-}a}$ dominates over the identity matrix.

Since, in this case, the matrix under inversion in Eq. (1) scales as $\exp(-2 \operatorname{Im} k_z h)$ and the rest scales as $\exp(-\operatorname{Im} k_z h)$, the amplification behavior is still present in general, in each element of t. The transmission t_{00} can be represented by Eq. (3) with the coefficients to the exponential replaced by smooth functions of ω and $\mathbf{k}$.

The second mechanism for enhancement of evanescent waves relies on a direct divergence in the overall transmission: i.e., an *overall resonance*. This is clear from the uniform medium case (2), whose denominator becomes zero when $1 - r_{p\text{-}a}^2 \exp(2ik_z h) = 0$, which is the condition for transverse guiding via total internal reflection. An evanescent incident wave can satisfy this condition exactly. It thus holds that a direct divergence can exist in the overall transmission of evanescent waves without any accompanying single-interface resonance, and therefore finite and strong amplification of evanescent waves results when the incidence wave does not exactly satisfy but is sufficiently close to this condition of overall resonance. In this case, there is no upper limit on the amplification and the transmission can even exceed that prescribed by Eq. (3); hence there is the potential to form an image provided that the correct degree of amplification is induced. These arguments are also valid in the general case (1), at or near the singular points of $1 - T_{\mathbf{k},p} r_{p\text{-}a} T_{\mathbf{k},p} r_{p\text{-}a}$ whose inverse occurs in the transmission. If we write the relation between the light frequency ω and wave vector $\mathbf{k}$ at these singular points as $\omega = \omega_0(\mathbf{k})$, then close to such a resonance the transmission t_{00} is described by

$$t_{00} = \frac{C_0(\omega, \mathbf{k})}{\omega - \omega_0(\mathbf{k})}, \tag{4}$$

where $C_0(\omega, \mathbf{k})$ is some smooth function of ω and $\mathbf{k}$. For a given ω, the issue is then to design photonic crystals with the appropriate dispersion relation $\omega_0(\mathbf{k})$ so that Eq. (4) approximates the required amount of amplification.

Both mechanisms of evanescent-wave amplification described here involve some divergences in the transmission process. Physically, such a divergence means that energy is being pumped indefinitely by the incident wave into both the transmitted and reflected fields, whose amplitudes increase in time without limit. Equivalently, a finite field inside the structure can be produced by zero incident field; i.e., it is a *bound* (guided) electromagnetic mode. In other words, a bound photon mode on the air/photonic-crystal surface (a surface state) leads to a single-interface resonance, and a bound photon state inside the slab leads to an overall resonance. In the overall resonance case, the dispersion relation of the bound photon mode is just $\omega = \omega_0(\mathbf{k})$ in Eq. (4). A similar equation can also be used to represent the zeroth-order term in $t_{p\text{-}a}$ close to a single-interface resonance:

$$t_{p\text{-}a,00} = \frac{C_{p\text{-}a}(\omega, \mathbf{k})}{\omega - \omega_{p\text{-}a}(\mathbf{k})}, \tag{5}$$

with the single-interface bound photon dispersion relation $\omega_{p\text{-}a}(\mathbf{k})$ and a smooth function $C_{p\text{-}a}(\omega, \mathbf{k})$. Both $C_{p\text{-}a}$ and C_0 here represent the coupling strength between the incidence wave and the respective bound photon state.

It is instructive to compare these two amplification mechanisms by their applicable ranges. As shown in Ref. 5, in an ideal material slab with $\epsilon(\omega_{sp}) = -1$ and $\mu(\omega_{sp}) = -1$, every evanescent wave is amplified by a single-interface resonance at the surface plasmon frequency ω_{sp}. For such a slab, $r_{p\text{-}a}$ diverges for any incident $\mathbf{k}$ and no overall resonance happens at the plasmon frequency. However, both ϵ and μ are necessarily dispersive,[7] and detuning from the single-interface resonance frequency we can satisfy the guiding condition

$$1 - r_{p\text{-}1}^2(\omega_\pm) e^{2ik_z h} = 0 \tag{6}$$

at two separate frequencies $\omega_\pm$, above and below ω_{sp}, reflecting the fact that the surface photon states on the two interfaces of the slab interact with each other, forming symmetric and antisymmetric combinations. In the general case, Eq. (6) can be satisfied and bound photon states inside the slab form even without the prior existence of interface states—i.e., without $r_{p\text{-}a}$ diverging. Thus both mechanisms may be available to amplify evanescent waves. To have a single-interface resonance in Eq. (1), it is required that the term associated with single-interface reflections dominate over 1. This can be expressed as

$$|\omega - \omega_{p\text{-}a}(\mathbf{k})| \ll |C_{p\text{-}a}| e^{-\operatorname{Im} k_z h}. \tag{7}$$

For an overall resonance, the condition becomes

$$|\omega - \omega_0(\mathbf{k})| \approx |C_0| e^{-\operatorname{Im} k_z h} \tag{8}$$

in order to produce an amplification magnitude similar to that in Eq. (3). We note that $C_{p\text{-}a}$ and C_0 are on the same order of magnitude if the bound photon modes inside the slab are constructed from combinations of the surface photon states. It is thus clear that in the general case, amplification of evanescent waves requires operation much closer to an exact resonance in the single-interface resonance mechanism than in the overall resonance mechanism. In addition, just like the situation near a surface photon state discussed previously, the overall resonance can in principle happen near a bulk-guided mode that is not evanescent inside the photonic-crystal slab. Put in another way, in general amplification is more easily achieved using an overall resonance than using a single-interface resonance. In the following, therefore, we make primary use of the second resonance mechanism and realize amplification of evanescent waves in the manner discussed here.

Amplification thus arises due to the coupling between the incident evanescent field and bound photon states of infinite lifetime, which usually exist below the light line.[40] In a periodic structure, the range of wave vector region below the light line is limited by the boundary of the surface Brillouin zone, due to Bragg scattering. What happens to the transmission of evanescent waves whose wave vectors are so large that they lie beyond the first surface Brillouin zone and become folded back into the light cone? In this case, the associated slab photon resonance mode changes from a *bound* state to a *leaky* state, and its frequency $\omega_0(\mathbf{k})$ becomes complex—i.e., $\omega_0(\mathbf{k}) \rightarrow \omega_0(\mathbf{k}) - i\gamma(\mathbf{k})$, with ω_0 and γ being real. This situation is actually described by the diagonal ele-

ment t_{nn} of t with $n \neq 0$ if we use n to index the surface reciprocal lattice vectors and assume $\mathbf{k}$ to be in the first surface Brillouin zone. When the incidence evanescent wave is sufficiently close to a leaky photon mode the transmission becomes

$$t_{nn} = \frac{C_0(\omega, \mathbf{k})}{\omega - \omega_0(\mathbf{k}) + i\gamma(\mathbf{k})}, \qquad (9)$$

which always has a finite magnitude. In principle, $|t_{nn}|$ can also reach values larger than unity provided that γ is small enough. However, as n goes away from 0 the spatial variation in the incident wave becomes more rapid. The leaky photon state, on the other hand, always maintains a constant field profile with variations on a fixed spatial scale, roughly that of each component in a cell of the crystal. Hence, for n sufficiently far from 0, C_0 in Eq. (9), determined by the overlap between the incident wave and the slab photon modes, must always approach zero and so must $|t_{nn}|$. Note that this is not true in the case of bound photon modes with $\gamma = 0$: amplified transmission may still occur if the incident wave is close to an exact overall resonance. The numerical results presented later in this paper indicate that, for the structure considered here, the transmission for evanescent waves coupling to leaky modes with $n \neq 0$ is *always* small and the possible amplification effect can be ignored.

It should be clear from this discussion that an amplified transmission of evanescent waves at a given ω and $\mathbf{k}$ is not restricted to materials with $\epsilon < 0$ or $\mu < 0$ only and can be achieved by coupling to bound photon states in general. Another interesting feature of this approach is that, as shown in Ref. 5, with the single-interface resonance-amplification mechanism, the reflection coefficient r can vanish, but in the overall-resonance mechanism here an amplified transmission process also implies an amplified reflected evanescent field in general. Since the latter mechanism is used in our numerical calculations below, most of the effects that arise due to the transmitted evanescent waves should also be expected in the reflected waves as well. These might lead to nontrivial consequences—for example, a feedback on the emitting source. In this paper, we assume that the source field is generated by some independent processes and ignore the potential influences of these effects.

III. PHOTONIC CRYSTAL SUPERLENSES

We now consider the problem of superlensing at a given frequency ω in photonic crystals. An ideal point source emits a coherent superposition of fields $\mathbf{F}_{source}(\mathbf{k})$ of different wave vectors $\mathbf{k}$, with $|\mathbf{k}| < \omega/c$ being propagating waves and $|\mathbf{k}| > \omega/c$ being evanescent waves. We place such a point source on the z axis (the optical axis) at $z = -h - u$ and observe the image intensity I_{image} in $z \geq 0$ to be

$$I_{image}(\mathbf{r}) = \left| \int d\mathbf{k} (\dots, \boldsymbol{\tau}_{\mathbf{k}} \exp(i\mathbf{k}_n \cdot \mathbf{r}_t), \dots) \cdot T_{\mathbf{k},a}(z) t(\mathbf{k}) T_{\mathbf{k},a}(u) \mathbf{F}_{source}(\mathbf{k}) \right|^2. \qquad (10)$$

In Eq. (10), $T_{\mathbf{k},a}(z)$ is the translation matrix in air that takes the fields through a distance z, $\boldsymbol{\tau}_{\mathbf{k}}$ is a polarization vector, $\mathbf{r}_t$ stands for transverse coordinates, $\mathbf{k}_n = \mathbf{k} + \mathbf{G}_n$, with $\mathbf{G}_n$ being the reciprocal vectors of the surface, and $\mathbf{k}_n$ is the transverse wave vectors in the air basis that we have been using. The brackets represent a row of polarizations and phases of the basis, and its dot product with the column vector of the transmitted field produces the complex field amplitude. The integral is carried out over the first surface Brillouin zone, and in the case of a uniform material it is over all $\mathbf{k}$'s in the transverse plane.

Conventional lenses only image the portion of the incident field with $|\mathbf{k}| < k_M$ for $k_M < \omega/c$, limited by the numerical aperture. A *perfect* lens,[5] made of left-handed materials with $\epsilon = -1$ and $\mu = -1$, not only focuses all propagating waves with negative refraction, but also amplifies all evanescent waves with $|\mathbf{k}| > \omega/c$, so that all Fourier components of the source field reappear perfectly in the image plane of geometric optics. One unusual aspect in such a scenario is that the fields in certain spatial regions become *divergent* and the associated energy density becomes infinite if the losses are ignored.[24] However, this observation merely reflects the fact that infinite-resolution imaging requires an infinite time interval to reach its steady state, and the original proposal[5] still

remains valid in the sense that arbitrarily fine resolution is in principle possible. Here, we use the term *superlens* to denote a negative-refractive slab that not only focuses all propagating waves by negative refraction without limitation of finite aperture, but also amplifies at least *some* evanescent waves in a continuous range beyond that of the propagating waves. In this context, *superlensing* refers to the unconventional imaging effects due to the presence of the additional near-field light. The phenomena considered here thus contain the main features of Ref. 5. In general, however, the magnitude of transmission will not reproduce exactly that for perfect image recovery, and the resulting image will be *imperfect* and possess quantitative aberrations. Below, we focus our attention on 2D situations where most of the quantities can be treated as scalars. We choose the transverse coordinate to be x and use unity for every G_n component of $F_{source}(k)$ for all k, appropriate for a point source in 2D.

Our starting point here is the focusing by negative refraction of all propagating waves with $k < \omega/c$ (AANR) (Ref. 12); a brief discussion of the behaviors outside the frequency range of AANR will be presented in Sec. V. With AANR, all propagating waves can be transmitted through the photonic-crystal slab with transmittance of order unity and produce a intensity maximum behind the slab; i.e., they focus into a
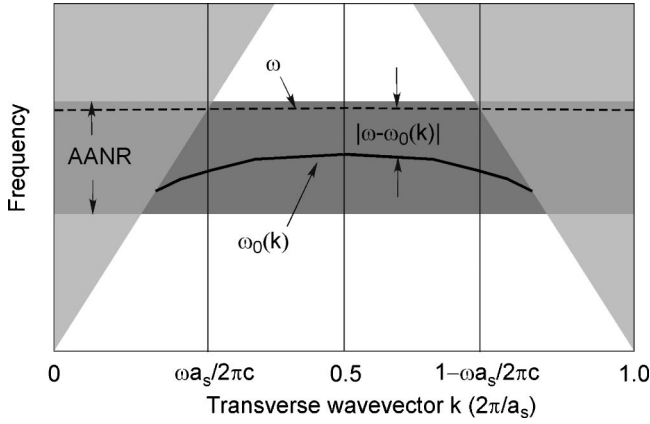
FIG. 2. Schematic illustration of amplification of evanescent waves and superlensing in photonic crystals. The light-shaded regions are the light cone, and the dark shaded region is the AANR frequency range. The curve marked $\omega_0(k)$ outside the light cone is a band of bound photon states inside a slab of photonic crystal. The dashed line marked ω indicates the operation frequency. Amplification requires that $|\omega - \omega_0(k)|$ be small for all $k > \omega/c$, especially the large k's, which in turn requires the $\omega_0(k)$ curve be "flat." In this repeated zone scheme, a bound photon state may only exist in the range $\omega/c < k < 2\pi/a_s - \omega/c$, which imposes an upper cutoff for superlensing using photonic crystals.

real image there. Superlensing requires amplified transmission for an additional range of transverse wave vectors, $\omega/c < k < k_M$. In Ref. 5, $k_M = \infty$. The important difference for superlensing with a photonic crystal is that k_M is in general finite. This is clear from the discussion in Sec. II, where a finite high cutoff to the transmission spectrum results as a consequence of Bragg scattering of light to leaky photon modes. This finite k_M makes the image reconstruction process through a photonic-crystal superlens no longer divergent even in the lossless case. Physically, the amplification of evanescent waves requires near-resonance coupling and the resulting growth of an approximate bound photon state during transmission. Amplification of larger k components thus requires exponentially higher energy density in the bound photon mode and an exponentially longer time interval to reach a steady state. Our numerical results below are mainly calculated in the frequency domain and therefore represent the steady-state behavior after the transients have died away in *finite* time.

To actually realize amplification of evanescent waves for $\omega/c < k < k_M$, one must design the photonic-crystal structure carefully so that Eq. (8) holds for *all* evanescent waves in this range. For large k, $k_z = +\sqrt{\omega^2/c^2 - k^2}$ has a large positive imaginary part, and therefore the operation frequency ω should be very close to the resonance frequency $\omega_0(k)$ of a bound photon state. This means that for large k, the dispersion relations $\omega_0(k)$ must approach a "flat" line near ω within the AANR range, as shown in Fig. 2. In general, there are two classes of bound photon modes within a photonic-crystal slab. One consists of those guided by the slab as a whole, similar to the guided modes in a uniform dielectric slab. The other class includes those guided by the air/slab surfaces; i.e., they are linear combinations of surface states,[30]

which decay exponentially both in air and in the slab away from the surface. Although both classes of bound modes can be employed to achieve amplification for a given k, most of the wave vector region $\omega/c < k < \pi/a_s$ within the AANR frequency range involves a partial photonic band gap and can only accommodate the surface photon states. Furthermore, the surface states of photonic crystals are known to depend on the fine details of the surface structure—e.g., the surface termination position in a given direction—and can be tuned to be any frequency across the band gap at least for a single k point.[30] Thus, the slab surface photon states are attractive candidates for achieving flat bound photon bands within the AANR range for superlensing. In our numerical example, we give one 2D design that meets this goal by simply adjusting the termination position of the crystal surface.

What is the ultimate limit to the imaging resolution of a photonic-crystal superlens? Following Ref. 5, we may interpret the image of a point source as an intensity peak within the constant-z plane of AANR focusing, and we can measure the resolution of such a peak by the distance between the nearest minima of this intensity peak. Taking into account the decay of the evanescent light as it travels in air from the source plane to the incidence surface of the slab and from the exit surface of the slab to the image plane, we can estimate the image field using a simplified model. In this model, we assume unit total transmission from the source to the image for $|k| < k_M$ and zero transmission for $|k| > k_M$. The intensity profile on the image plane then reads

$$I_{image}(x) = \left| \int_{-k_M}^{k_M} e^{ikx} dk \right|^2 = \frac{4 \sin^2(k_M x)}{x^2}, \qquad (11)$$

which has a peak amplitude at $x = 0$ with a transverse size $\Delta = 2\pi/k_M$—i.e., the distance between the first zeroes around the peak. This image size is zero in a material with $\epsilon = -1$ and $\mu = -1$, since $k_M = \infty$, leading to the interpretation of a "perfect" image. At present in a photonic crystal, quantitative estimates of the minimum possible Δ (i.e., maximum possible k_M) may be obtained by looking at Fig. 2. In the best situation, all the surface modes with $k < 0.5(2\pi/a_s)$ can be used directly for amplification if they satisfy (8),[41] which gives $k_M \geq 0.5(2\pi/a_s)$. Since this estimate ignores the strong Bragg-scattered wave components in the surface states near the surface Brillouin zone edge, it is a conservative estimate. From Fig. 2, we also deduce the maximum wave vector of a "flat" surface band below the light line that can be coupled to at frequency ω to be $(1 - \omega a_s/2\pi c)(2\pi/a_s) = 2\pi/a_s - \omega/c$, which is an overestimate. Putting these results together, we thus obtain the ultimate resolution limit of a photonic-crystal superlens to be

$$\frac{a_s \lambda}{\lambda - a_s} < \Delta < 2a_s. \qquad (12)$$

According to the Rayleigh criteria, the minimum feature size that can be resolved by such a device is $\Delta/2$. Thus, the resolution of a photonic-crystal superlens at a single frequency is only limited by its surface period a_s instead of the wavelength of operation λ; i.e., superlensing is in general possible
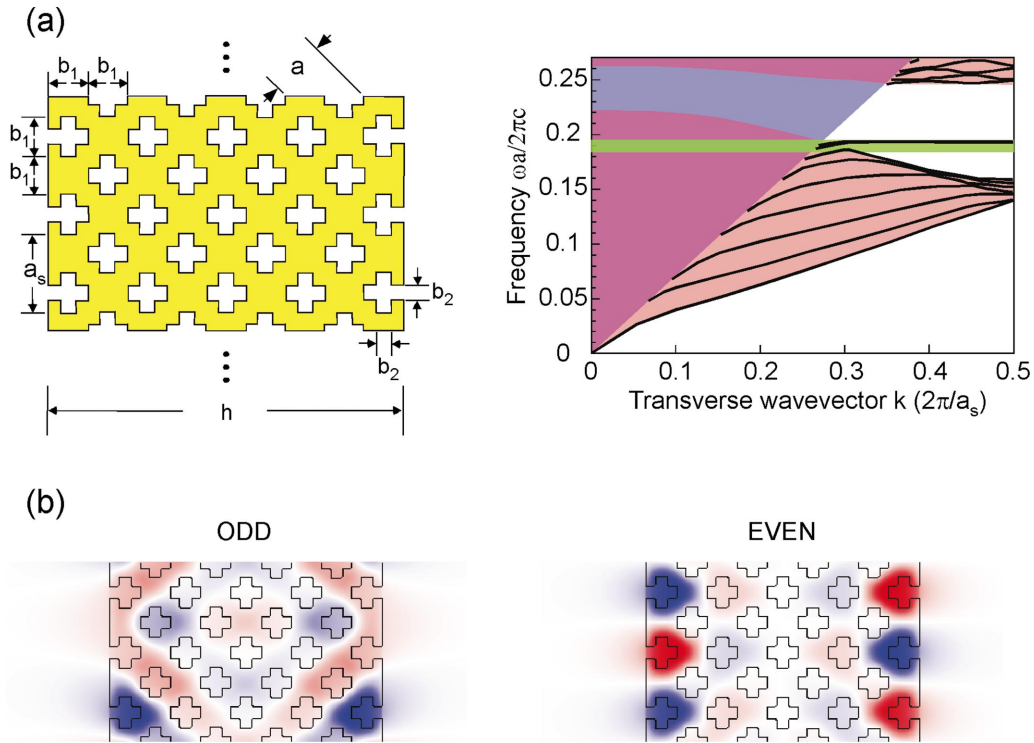
FIG. 3. (Color) Bound photon modes with TE (magnetic field perpendicular to the plane) polarization in a 2D photonic crystal slab. (a) Left panel: the actual photonic crystal used in calculation. The parameters are $a_s = \sqrt{2}a$, $b_1 = 0.5a_s$, $b_2 = 0.2a_s$, and $h = 4.516a_s$. Right panel: the calculated band structure of bound photon modes (black curves), plotted on top of the photonic band structure projected along the surface direction (the red-filled region). The blue-filled region indicates the light cone. The green range is the frequency range for AANR in this photonic crystal. (b) Distribution of the magnetic field perpendicular to the plane for the surface photonic modes at $k = 0.45$ $(2\pi/a_s)$. Left and right panels represent odd and even symmetries with respect to the mirror plane at the center of the structure. Red and blue indicate positive and negative values of the magnetic field.

in a positive-index photonic crystal. Our considerations also give a guideline for designing high-resolution superlenses: for a given wavelength, the smaller a_s—i.e., the lower in the band structure one operates with AANR—the better the resolutions will be. In principle, by using sufficiently large dielectric constants in its constituents, a photonic-crystal superlens can be designed to operate at a wavelength arbitrarily larger than a_s. A similar superlensing trend[42] is also achievable using localized plasmon polariton resonances in metallic photonic crystals,[43,44] in accordance with known results in the left-handed materials. If, furthermore, a sufficiently flat surface band is achieved in the AANR frequency range of such a photonic-crystal slab by manipulating its surface structures, imaging arbitrarily exceeding the diffraction limit is possible. Therefore, there is no theoretical limit to superlensing in photonic crystals in general. In practice, of course, available materials, material losses, and unavoidable imperfections in surface structures will limit the performance of such superlenses.

It must be noted that the image of a superlens considered above is substantially different from the conventional real image of geometric optics. Conventional real optical images always correspond to an intensity maximum: i.e., a peak of the field amplitude distribution both in x and z directions. When only the propagating waves are transmitted through the superlens, they similarly produce an intensity maximum in $z > 0$: i.e., the image of AANR. The position of this image

may be simply estimated by paraxial geometric optics around the z axis. However, when evanescent waves are included, they bring distortions to the image and the resulting intensity maximum is no longer at the position of the AANR image. A simple illustration of the image pattern is provided by our simplified cutoff model. The full expression of the image in this model with a high cutoff $k_M > \omega/c$ can be written as

$$I_{image}(x,z) = \left| \int_{-\omega/c}^{\omega/c} e^{ikx + i\sqrt{\omega^2/c^2 - k^2}(z - z_0)} dk \right.$$
$$\left. + \left(\int_{-k_M}^{-\omega/c} + \int_{\omega/c}^{k_M} \right) e^{ikx - (\sqrt{k^2 - \omega^2/c^2})(z - z_0)} dk \right|^2,$$

(13)

where $z = z_0$ is assumed to be the focusing plane of AANR. Inside the absolute value sign of Eq. (13), the first term has constructive interference at $z = z_0$ and represents an intensity maximum there, but the second term always displays asymmetric amplitude distributions in z across $z = z_0$. Thus, for $k_M > \omega/c$ the overall intensity distribution no longer has a maximum at $z = z_0$. The detailed image pattern has a sensitive dependence on the interplay between the propagating and evanescent waves.

For k_M slightly above ω/c, the strength of evanescent waves is comparable to that of propagating waves. An intensity maximum still exists in the region $z>0$, but is shifted away from $z=z_0$ toward the lens. This intensity maximum thus appears as a real image similar to conventional optics. Note that in general it will have a transverse size that is a little bit smaller than $2\pi/k_M$—i.e., the transverse size of the peak in the plane $z=z_0$. Since this situation is for k_M slightly above ω/c, it may be called the *moderate subwavelength limit*, and the transverse size of an intensity maximum is always limited by a fraction of the wavelength.

When k_M exceeds a certain threshold, the evanescent waves begin to dominate the image pattern. In this situation, an intensity maximum completely disappears in the region $z>0$, where the optical intensity becomes monotonically decreasing. We estimate the k_M threshold for this behavior to be about $k_{M,th}=1.35\omega/c$, with a transverse size of the intensity maximum about half a wavelength at this threshold, using the simplified model (13). This crude qualitative estimate will be confirmed in our numerical calculations. The case of superlensing with $k_M>k_{M,th}$ can thus be called the *extreme subwavelength limit*. From another viewpoint, at $\omega/c\ll k_M$ we have $\lambda\gg a_s$, and if we also assume that the slab thickness h is small compared to λ, then the system may be regarded to be in the near-static limit. The absence of an intensity maximum in $z>0$ may then be understood simply by the elementary fact that in electrostatics and magnetostatics potentials can never reach local extrema in a sourceless spatial region. Thus, in the extreme subwavelength limit the imaging effect of a superlens is strictly in the transverse direction only. Compared to a conventional lens, which generally has a power-law decaying intensity distribution away from its image, the superlens has a characteristic region between the superlens and the image where an exponentially growing intensity distribution exists.

A related effect of evanescent waves on the image is that, for $k_M>\omega/c$, the image intensity is generally larger than that for $k_M\lesssim\omega/c$. This occurs in the simplified model (13) due to the addition of evanescent-wave components. Note also that, in this model, no exact resonant divergence is present in the transmission and the intensity enhancement effect is prominent in the region between the slab and image plane of geometric optics. A more general situation occurs when the operating frequency ω falls inside the narrow frequency range of the bound photon states, so that a distinct number of bound mode with near-zero group velocities can be excited on exact resonance. The contribution from one such exact resonance pole at $\omega=\omega_0(k_0)$ to the transmission may be estimated as

$$\int dk \frac{C_0(\omega,k)}{\omega_0(k_0)-\omega_0(k)} \approx \frac{1}{(\partial\omega/\partial k)|_{k=k_0}} \int dk \frac{C_0(\omega,k)}{k_0-k}.$$

(14)

The integral over k, though not suitable for analytical evaluation in general, can usually be regarded as having a finite principal value and depends on the detailed behavior in $C_0(\omega,k)$. The influence of each pole on the transmitted image can be thus seen to be inversely proportional to the group
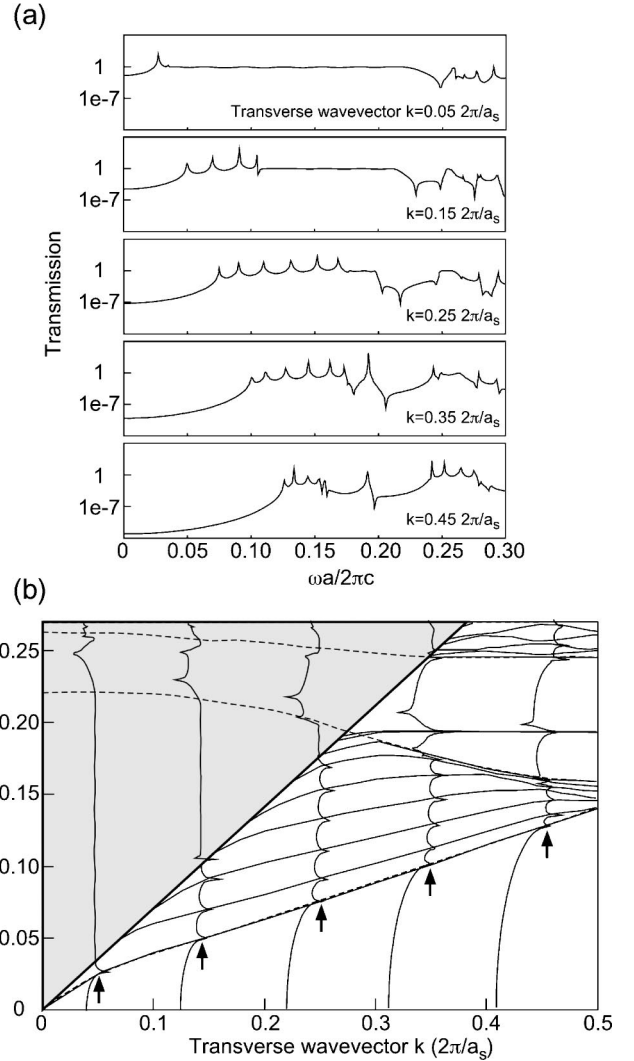

FIG. 4. Frequency spectrum of transmission and links to bound slab photon modes. (a) Zeroth-order transmission ($|t_{00}|^2$) through the photonic-crystal slab in Fig. 3 for various transverse wave vectors, plotted on a logarithmic scale vs frequency. (b) The transmission curves in (a) are plotted on the bound photon band structure of the photonic-crystal slab [Fig. 3(a)]. The arrows indicate the transverse wave vector for each transmission curve. The shaded region is the light cone.

velocity of the bound photon state at the resonance and is strongest for modes with the smallest group velocities. When operating on exact resonance to the flat surface bands with very small group velocities, the field pattern in a wide spatial region in $z>0$ that extends beyond the image may be dominated by the surface states, often with extraordinary strength. Thus, we can call this regime of superlensing *enhanced surface resonance*. On the one hand, such an effect might be useful in applications where a large field amplitude is desired. On the other hand, since a surface resonance is a *delocalized* field distribution, there is very little information contained within the intensity distribution about the transverse location of the source in this case. This is a subtle point to be avoided in imaging applications.

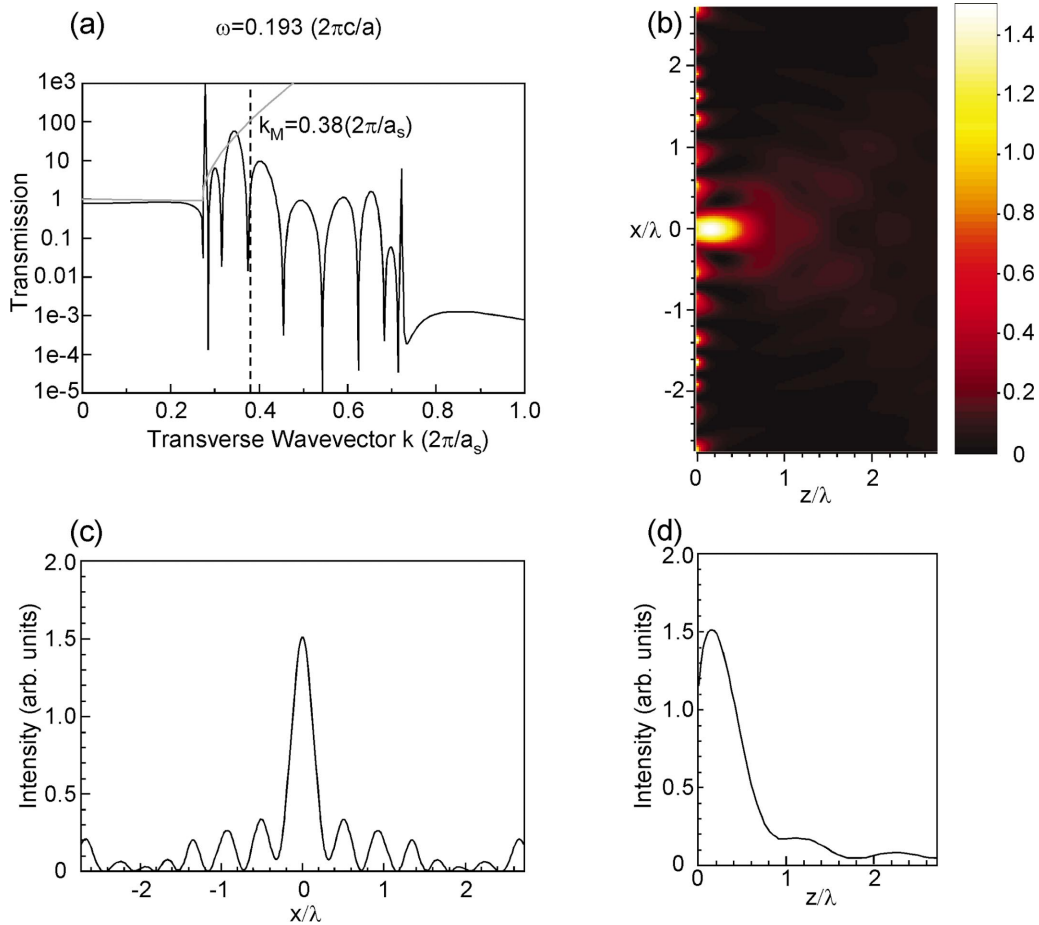In many experimental situations, light intensity is the

FIG. 5. (Color) Transmission and intensity distribution in the image space for $\omega=0.193\ (2\pi c/a)$, for a photonic crystal slab in Fig. 3 illuminated with an ideal point source. (a) Zeroth-order transmission $[|t_{00}|^2$ for $k<0.5(2\pi/a_s)]$ plotted on a logarithmic scale vs the incident transverse wave vector. The gray curve indicates the transmission value for perfect image reconstruction at the AANR focusing position of the present slab. The effective high cutoff of the transverse wave vector k_M is marked out in dashed lines. (b) The intensity distribution in real space to the right of the slab for $z>0$. The right surface of the slab is at $z=0$. (c) The data in (b) plotted in the plane of $z=0.6a_s$ $=0.16\lambda$—i.e., through an intensity maximum. (d) The data in (b) plotted with $x=0$—i.e., on the z axis.

quantity that is responsible for most physical effects and can be measured directly. Both the subwavelength transverse resolution and the spatial region of extraordinarily high intensity can thus serve as direct experimental evidence of superlensing. From the viewpoint of applications, imaging in the transverse direction alone below the diffraction limit is sufficient and desirable for many situations, such as sensing and detecting or strong focusing for active phenomena. Our considerations indicate the possibility of a variety of image patterns impossible in conventional geometric optics in the image of a superlens, based on the interplay between near-field and far-field light. With a photonic crystal, a flexible superlens may be constructed in which all of these physical effects are readily observable.

IV. NUMERICAL RESULTS

In this section, we present numerical results that confirm the above discussion on superlensing in photonic crystals. The main crystal structure we choose to study is a square lattice of two overlapping rectangular air voids in a *lossless*

dielectric $\epsilon=12$, oriented along the (11) direction and with the various sizes specified in Fig. 3(a). The lattice constant of the square lattice is a, and the surface lattice constant is a_s $=\sqrt{2}a$. This configuration possesses a similar infinite-crystal band structure to the one studied in Ref. 12. Since it is a layered structure along the (11) direction, this crystal structure also allows for efficient numerical computations of transmission through a finite slab in the frequency domain. For brevity, we assume a TE (magnetic field perpendicular to the 2D plane) polarization in all our calculations in this paper, and similar results can be expected for TM modes as well.

A. Surface band structure

The band structure of the bound photon states on the photonic-crystal slab suspended in air with (11) surface termination is calculated by preconditioned conjugate-gradient minimization of the block Rayleigh quotient in a plane-wave basis[45] using the supercell approach. The results are presented in Fig. 3(a). Below the light cone and inside the re-
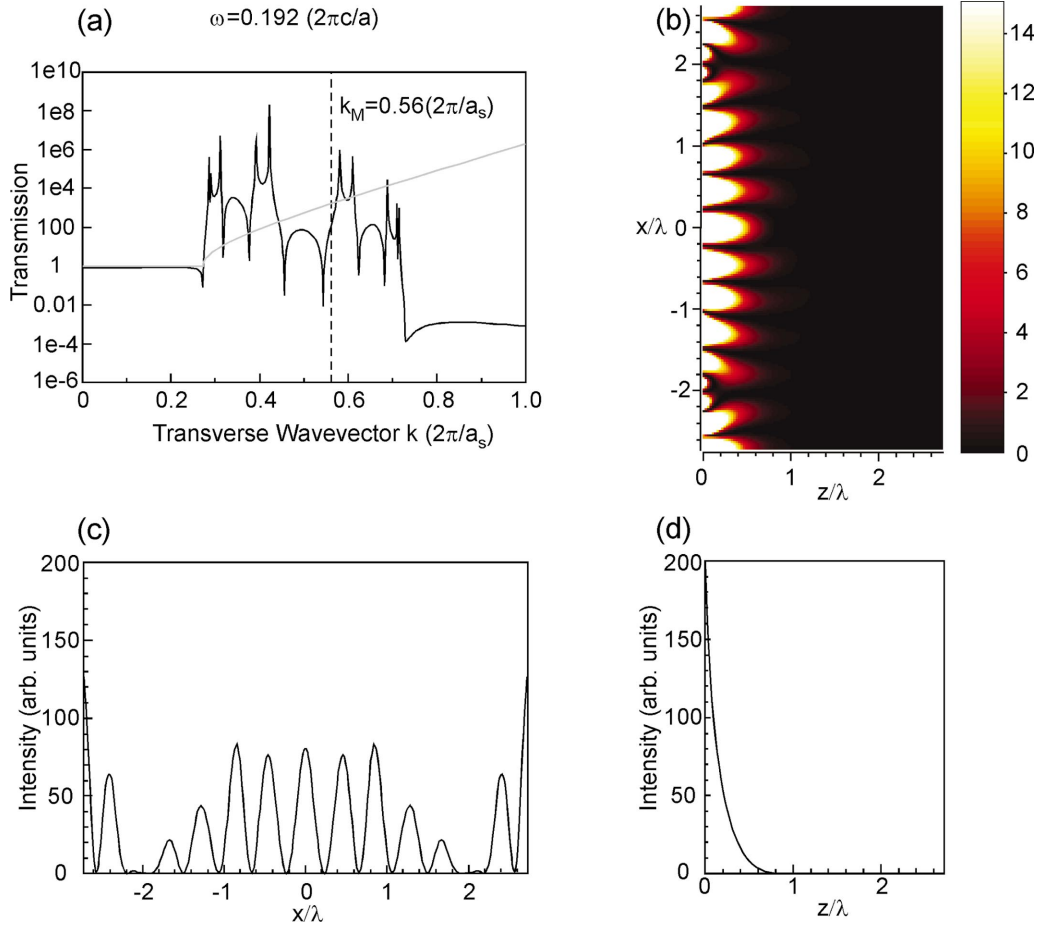
FIG. 6. (Color) Numerical results similar to those shown in Fig. 5 for $\omega = 0.192 \ (2\pi c/a)$. (c) is a plot in the plane of $z = 0.6a_s = 0.16\lambda$ (not through an intensity maximum).

gion of projected band structure of an infinite crystal, the modes are bound photon states guided by the slab as a whole; the modes inside the partial photonic band gap are the surface states guided around the air/slab interfaces in this photonic crystal. The field profiles of the symmetric and antisymmetric combinations of the surface modes on the two surfaces with respect to the mirror symmetry plane are also shown in Fig. 3(b). Deep in the gap where the confinement is strong, the splitting between these two bands becomes small and the two bands merge into one curve in Fig. 3(a). The crystal thickness h and its associated surface termination position are chosen so that the frequencies of the surface modes lie inside the AANR frequency region with little dependence on the transverse wave vector k—i.e., two flat, nearly degenerate bound photon bands near the frequency $\omega = 0.192(2\pi c/a)$. This situation thus approximately realizes that in Fig. 2 and is well suited to achieve superlensing.

B. Transmission spectrum

The transmission calculations for arbitrary frequency ω and wave vector k have been performed in the scattering-matrix approach under Bloch periodic boundary conditions, such as that of Whittaker and Culshaw for patterned layer photonic structures.[46] To compare the results with those obtained from eigenmode computation by plane-wave expansion, we fix the incident wave vector and calculate the frequency spectrum of the transmission. The transmission is presented on a logarithmic scale in Fig. 4(a). The pronounced peaks in the transmission indicate resonant excitation of the bound photon states by the incident radiation, and they approach infinity in the limit of continuous numerical sampling points in frequency. From the comparison between the transmission peaks and the surface band structure in Fig. 4(b), we find excellent agreement between the two numerical methods. Near each resonance, the transmission of evanescent waves reaches large amplification values well exceeding unity, providing the basis of superlensing.

An unusual feature to notice in the transmission spectrum, not expected in a uniform negative-index slab, is the presence of zeros in the transmission when the frequency is in the photonic band gap. These zeros occur as sharp dips on the spectrum, and the number of these dips increases with the slab thickness in a manner suggestive of Fabry-Perot interferences. However, they cannot be explained by the conventional Fabry-Perot interference, which only occurs in the denominator of Eq. (2) and never leads to a zero. Instead, they occur as a result of interference between the different evanescent eigenmodes of the photonic crystal in Eq. (1), coupled together through the phase matrix $T_{\mathbf{k},p}$. Zeros occur
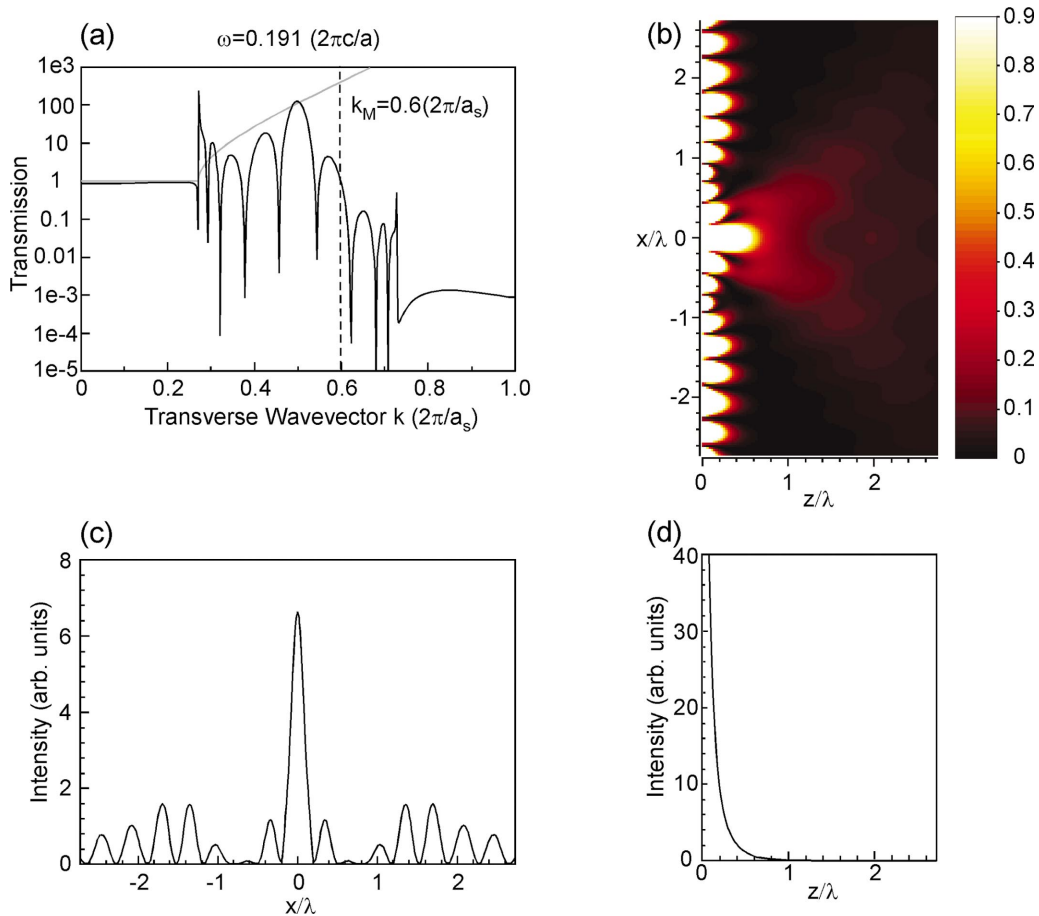
FIG. 7. (Color) Numerical results similar to those shown in Fig. 5 for $\omega = 0.191$ $(2\pi c/a)$. (c) is a plot in the plane of $z = a_s = 0.27\lambda$ (not through an intensity maximum).

because inside a photonic band gap, several eigenmodes can have equal amplitude and cancel each other exactly. These zeros are apparently quantitative new features in the transmission spectrum, but since they are only at a discrete number of frequency points, they do not change the qualitative structure of imaging. The quantitative effects of transmission zeros are included in the numerical results of superlensing in the next section.

C. Image patterns of a superlens

We calculate the transmission as a function of incident wave vector k at a fixed frequency ω close to that of the surface modes, using the method of Sec. IV B. The complex transmission data for these plane waves are then summed at each z values as in Eq. (10) to obtain the image pattern from a point-dipole source placed on the z axis at $z = -h - u$. Here $u = 0.1a_s$ is used in these calculations, and the k sampling points range from $k = -5(2\pi/a_s)$ to $k = 5(2\pi/a_s)$ in steps of $0.001(2\pi/a_s)$, to model the continuous range of $-\infty < k < \infty$. This finite resolution roughly corresponds to a finite transverse overall dimension of the structure of 1000 periods and is sufficient for illustrating the various appearances of the image.[47] Our results are summarized in Figs. 5, 6, and 7. The frequency of operation is shifted by only $0.001(2\pi c/a)$ from one figure to the next. In the all cases

here, the transmission for propagating waves is nearly the same and close to unity. However, large differences in the field patterns for $z > 0$ can be observed in the results, indicating that a fine control over the transmission of evanescent waves is possible.

For $\omega = 0.193(2\pi c/a)$ (Fig. 5), the operation frequency is outside the frequency range of the "flat" surface bands. The transmission results in Fig. 5(a) show smooth behavior throughout the range of wave vectors and exhibit zeros as noted in Sec. IV B. Notice that the magnitude of transmission oscillates around order unity for the evanescent waves for $0.27(2\pi/a_s) < k < 0.73(2\pi/a_s)$, but for $k > 0.73(2\pi/a_s)$ the transmission drops precipitously to a low level below 1×10^{-3}. This confirms our previous expectation that the "flat" bound photon band below the light cone ($0.27 < ka_s/2\pi < 0.73$) should lead to amplified transmission of evanescent waves and that the amplification effect should disappear when the evanescent wave is coupled back into the continuum. In the calculated image shown in Fig. 5(b), a clear intensity maximum at $x = 0, z = 0.6a_s = 0.16\lambda$ in free space can be observed. Quantitative cross sections of this maximum in both the x and the z axes are shown in Figs. 5(c) and 5(d), respectively. The transverse x size of this peak is $0.66\lambda < \lambda$, demonstrating that the contribution of evanescent waves to imaging is comparable to that of propagating
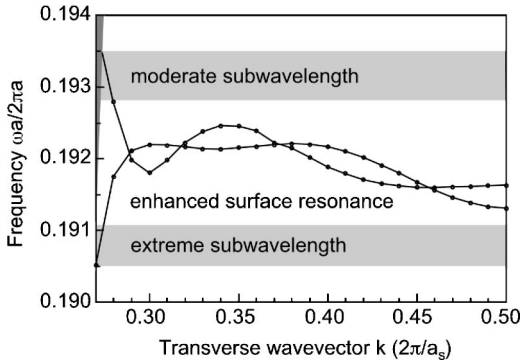
FIG. 8. The detailed surface band structure and its influence on subwavelength imaging. The solid circles are the divergence peaks in the calculated transmission through the structure in Fig. 4. The dark-shaded area in the upper left corner is the light cone. The frequency range for imaging with none or moderate subwavelength contribution is from 0.1928 to 0.1935. The frequency range for extreme subwavelength superlensing is from 0.1905 to 0.1911. The region between them is the region of the flat surface bands for enhanced surface resonance. The sequence of these three frequency ranges here are due to the particular shape of the surface bands and can be different in other systems.

waves. This situation, however, still possesses an intensity maximum and is therefore in the moderate subwavelength regime. The imaging pattern is similar to what we obtained previously using the finite-difference time-domain (FDTD) method,[12] in which an intensity maximum was identified with the location of a real image. Meanwhile, in the present case, the geometric image location of AANR calculated from constant-frequency contours of this photonic crystal is at $z = 1.4a_s = 0.38\lambda$. In the constant-z plane of the AANR image, the intensity distribution in x is similar to that in Fig. 5(c), with a transverse size $\Delta = 0.71\lambda$. This value corresponds to an effective high cutoff $k_M \approx 1.4\omega/c = 0.38(2\pi/a_s)$, which is close to the threshold k_M value in the simplified model obtained in Sec. III. For the present position of the AANR image, we plot the amplification required to restore the source *perfectly* in gray lines in Fig. 5(a), which can be compared to the actual transmission data and the effective cutoff k_M. Although the imaging is not perfect, the range $\omega/c < k < k_M$ roughly indicates the interval in which the actual transmission follows the behavior in the ideal case. Since k_M is actually larger than the wave vectors of several transmission zeros in the spectrum, we have confirmed that these zeros do *not* have a significant influence on superlensing.

If ω is decreased slightly to $\omega = 0.192(2\pi c/a)$ (Fig. 6), the frequency falls inside the narrow range of the surface mode frequencies. The transmission increases dramatically, and pairs of peaks in the transmission spectrum occur, representing excitation of surface mode combinations of even and odd parity. These surface modes have large amplitudes, as evidenced by the compressed color table in plotting Fig. 6(b) and the exponential decay of intensity along z axis in Fig. 6(d), and they now completely dominate the image. In accordance with our discussion before, the focusing effect of propagating waves becomes insignificant against this strong background. If the field distribution in a plane of constant z

is measured, an example shown in Fig. 6(c), many closely spaced, near-periodic strong peaks occur, in striking contrast to the familiar appearance of a focused optical image. Here, this pattern of intensity distribution persists for increasing z in the near field and even appears on the focusing plane of AANR $z = 1.1a_s = 0.31\lambda$. Due to the exponential decay of intensity along the z axis and the *delocalized* field distribution in the transverse direction, neither the z coordinate nor the transverse location of the source can be easily retrieved from this image pattern. The present image field pattern is hence undesirable for imaging purposes and should instead be exploited in situations where enhanced intensity in an extended spatial region is preferred. We infer the effective cutoff wave vector by the width of the central peak $\Delta = 1.8a_s = 0.49\lambda$ on the plane of AANR image, and obtain $k_M = 0.56(2\pi/a_s)$, as marked out on Fig. 6(a) where the transmission curve for *perfect* image reconstruction is also plotted. It is evident that the actual transmission deviates significantly from the ideal case, which explains the nonfocused image pattern.

An image pattern with intermediate behavior between these two situations can occur, for example, if we take ω to be $\omega = 0.191(2\pi c/a)$ (Fig. 7). This frequency is outside the "flat" surface band frequency range, and consequently the transmission becomes smooth again. Amplified evanescent waves are still present in the image space, which create an exponentially decaying intensity profile along the z axis as shown in Fig. 7(d). In contrast to the case in Fig. 6, a distinct intensity peak can now appear within a plane of constant z shown in Fig. 7(c), with a size significantly smaller than the wavelength. Here we have actually achieved $\Delta = 0.45\lambda$ at $z = a_s = 0.27\lambda$, approximately the same location as predicted by AANR. This image size is in accordance with the general prediction of Eq. (12) where $a_s\lambda/(\lambda - a_s) = 0.37\lambda$ and $2a_s = 0.54\lambda$ for the present photonic crystal. We infer the high cutoff wavelength k_M in this case to be $k_M = 2.2\omega/c = 0.6(2\pi/a_s)$, which corresponds to the extreme subwavelength limit. In this limit, there is no intensity maximum in $z > 0$, consistent with our previous expectation, and the calculated transmission for $k < k_M$ also displays roughly the same trend in k dependence as the ideal transmission for perfect image recovery. We have therefore found a superlensing image pattern quite similar to that considered in the original perfect lens proposal,[5] in the present case with an upper cutoff, without requiring negative-index materials.

To summarize, these computational results establish that superlensing is possible with carefully designed photonic crystals and exhibit large modifications to the image field distribution due to the presence of evanescent light. To preserve an intensity maximum in the image space, only a modest amount of evanescent waves can be included in the moderate subwavelength regime, and the resolution of the resulting intensity maximum is limited by a fraction of the wavelength (Fig. 5). Alternatively, it is also possible to enhance the transmission of evanescent waves to such an extent that they dominate over propagating waves (Fig. 6). In this case of enhanced surface resonance, a focused image disappears completely and the field distribution becomes that of the resonantly excited, delocalized surface modes. Furthermore, a scenario qualitatively similar to that of a left-hand
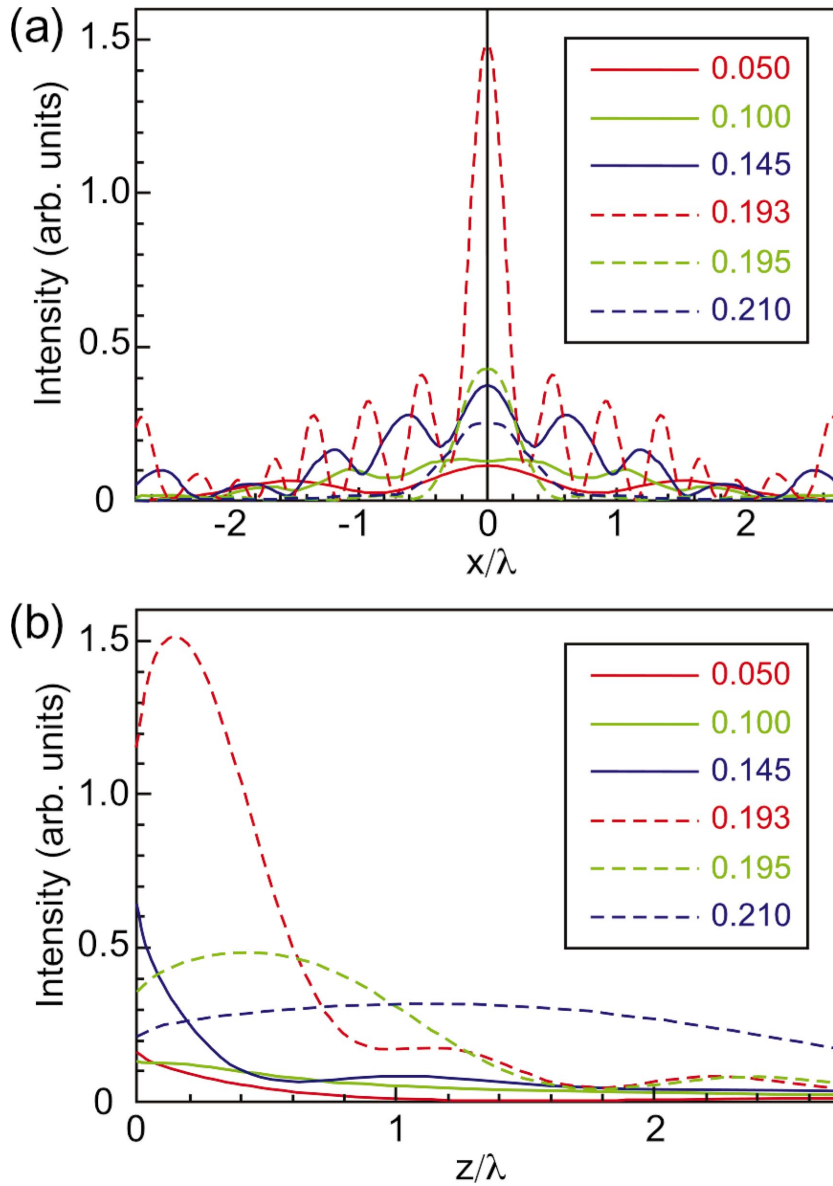
FIG. 9. (Color) Numerical results of the imaging for various frequencies throughout the first photonic band for the structure in Fig. 3. (a) Intensity distribution along the transverse direction, commonly measured at $z=0.5a_s$ for several frequencies shown as insets. This z value is chosen for exhibition of large near-field effects at certain frequencies [e.g., $\omega=0.145(2\pi c/a)$]. The transverse intensity distribution at larger z values has a similar-shaped background but weaker near-field modulations. (b) Intensity distribution along the z axis for the shown frequencies. In both panels the inset numbers are the frequencies corresponding to each curve, in units of $(2\pi c/a)$.

material with $\epsilon=-1$ and $\mu=-1$ can be obtained (Fig. 7), with an evanescent field distribution containing a localized intensity peak in the focusing plane of AANR. The minimum size of this peak in this extreme subwavelength regime is limited only by the surface periodicity of the photonic crystal and not by the wavelength of light and is in principle only limited by the refractive index. Finally, our calculations indicate that in the present structure, each of these image patterns can appear in a narrow frequency range inside that of AANR, as indicated in the detailed surface band structure in Fig. 8. We conclude that the intensity distribution of the optical image formed by a superlens depends sensitively on the detailed balance between propagating and evanescent waves and can be tuned with great flexibility in photonic crystals.

V. DISCUSSION

For completeness, we show in Fig. 9 the calculated near-field intensity distributions in $z>0$ for a point source of vari-

ous frequencies throughout the first photonic band, with all other parameters the same as those in Sec. IV C. It is clear that for frequencies lower than the AANR range ($\omega=(0.050,0.100,0.145)(2\pi c/a)$), since most of the propagating waves do not experience negative refraction and are not focused, a broad background peak is always present in the transverse direction. An interesting feature to observe is that $\omega=0.145(2\pi c/a)$ is close to the band edge where there are many flat bands of guided photon bound modes that can be resonantly excited. Consequently, significant subwavelength surface resonance features appear on the broad background behind the slab. However, the overall resolution is now determined by the background, which is spatially broad and does not correspond to a subwavelength imaging effect. For frequencies above the AANR range ($\omega=0.195,0.210(2\pi c/a)$), since some of incident propagating radiation from air will experience total external reflection, the transverse resolution is always limited to be larger than or equal to the operating wavelength. All these can be com-
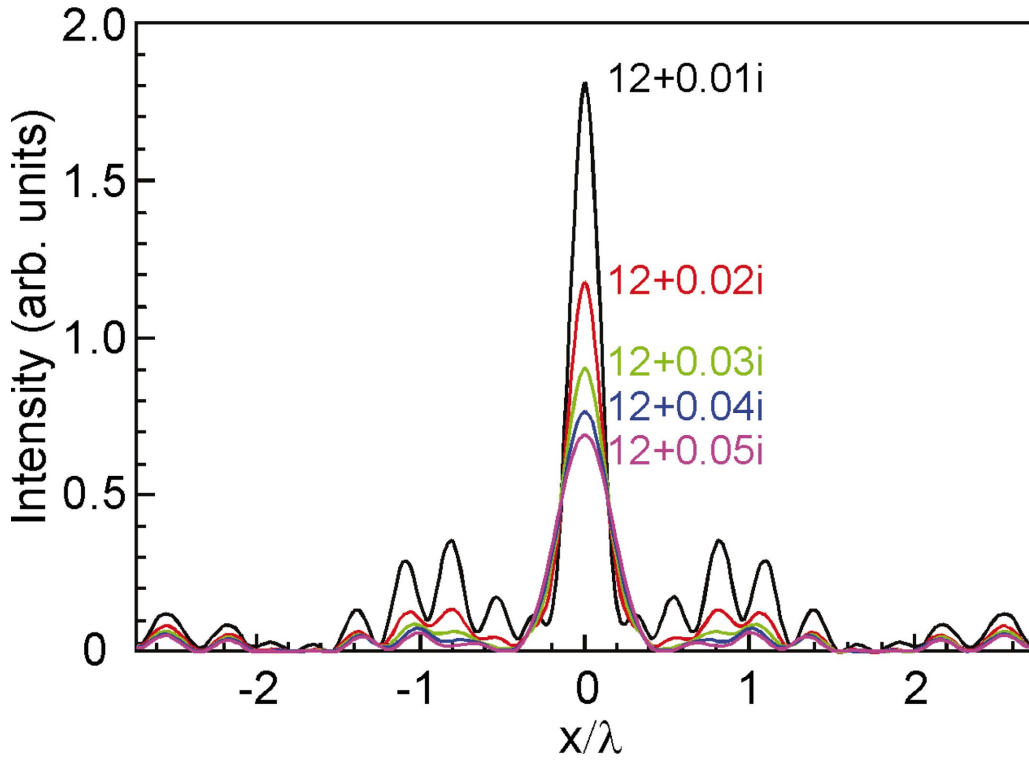
FIG. 10. (Color) Calculated transverse intensity distribution for imaging with lossy photonic crystals. Each inset number corresponds to the permittivity of the dielectric host for the curve of the same color. The crystal and point source are otherwise identical to those in Fig. 7. The intensity is plotted in the plane $z = a_s$ at the frequency $\omega = 0.191(2\pi c/a)$.

pared to $\omega = 0.193(2\pi c/a)$ where the extraordinary super-lensing enhancement in both the imaging resolution and intensity is shown. From this analysis, we conclude that *the only frequencies at which one can observe superlensing are inside the AANR range and close to a flat surface band.*

The above discussion has focused on ideal situations with no material absorption of light or structural imperfections. In practice, material losses are always present, which means that no transmission considered here will be truly infinite. In general, appreciable material losses will impose severe limitations on the transmission coefficient of evanescent waves, in a manner similar to that of the intrinsic energy leakage rate of a crystal mode above the light line, which in turn reduces the superlensing effect. However, it is also expected that, in the limit of extremely small material loss, in the sense implied by the original proposal of perfect lens,[5] our findings about the image of a superlens will remain valid. As an example, we show the calculated focusing effect in slightly lossy photonic crystals in Fig. 10. The losses are modeled as a positive imaginary part on the permittivity ϵ of the dielectric host, and results are calculated at the extreme subwavelength frequency $\omega = 0.191(2\pi c/a)$ for ϵ starting from $\epsilon = 12 + 0.01i$ up to $12 + 0.05i$. As the losses increase, the strength of the transmitted near fields is attenuated, and the subwavelength features in the central image peak gradually disappear. It is clear that a resolution at or below $\Delta = 0.5\lambda$ for a localized intensity peak in x is still achievable if $\epsilon \leq 12 + 0.01i$. The effects of surface imperfections on subwavelength imaging can also be qualitatively analyzed. We consider these defects to occur only on a length scale that is

smaller than a lattice constant and, thus, much smaller than the operating wavelength, with correspondingly little influence on propagating waves. Since the transmission of evanescent waves depends sensitively on the bound surface photon states, which in turn depend sensitively on the surface structure, imperfections are expected to be most influential on the crystal surface. Their effects may thus be minimized by improving the surface quality. Another kind of structural imperfection is a finite lateral size of the crystal. We have applied the FDTD method to such finite systems and found that, for a 20-period-wide slab, a focusing resolution around $\Delta = 0.6\lambda$ can be still obtained. These considerations suggest that the effects described in this paper should be observable in realistic situations.

Our discussion on the image of a 2D superlens can be put to experimental verification in a manner similar to that suggested in Ref. 12. Because the superlensing occurs in the first photonic band, it should also be directly applicable to 2D photonic-crystal systems suspended in 3D.[48] A more interesting extension of these phenomena would be to a full 3D system, which requires much more intensive computation for numerical modeling. For example, in 3D the resolution of focusing with infinite aperture but without evanescent waves is still limited by the wavelength λ, while the surface periodicity discussed in Eq. (12) should be replaced by the reciprocal of the minimum radius of the surface Brillouin zone. We show here in Fig. 11 the results of the computed bound photon modes of a slab of a 3D photonic crystal proposed in Ref. 15. As discussed in detail there, this photonic crystal enables AANR in full 3D and is most effective for waves
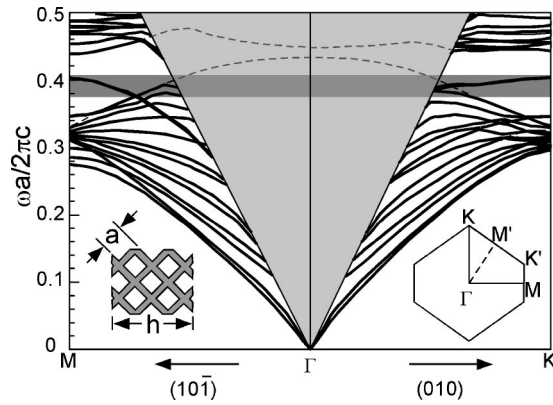
FIG. 11. Bound photon modes and projected band structure for a 3D photonic crystal capable of AANR. The solid lines are bound photon modes, and the dashed lines are the outlines for projected photonic band structure on the surface Brillouin zone. The light-shaded region is the light cone. The dark-shaded range is the AANR frequency range. A cross section of the crystal and the surface Brillouin zone are shown as insets. The thickness of the photonic-crystal slab is $h = 3.47a$.

polarized along $(10\bar{1})$. The surface band structure along ΓK and ΓM computed here, complicated as it may seem at first sight, bears a striking similarity to the TE and TM slab polariton bands of a dispersive negative-index materials calculated by Ruppin[49,50] when the direction of light polarization is taken into account. For the particular surface termination shown in Fig. 11, it is possible to obtain surface states within the AANR range of this photonic crystal. Since there is still a vast amount of freedom in tuning the fine details of the crystal surface structure without breaking the periodicity, it can be further expected that particular designs exist which lead to flat surface bands and can enable superlensing in full 3D. This tunability and flexibility in our approach should make photonic crystals a powerful and beautiful candidate in manipulating and focusing light on subwavelength scales, especially in the optical regime.

VI. CONCLUSIONS

In conclusion, we have explained the principles of the amplified transmission of evanescent waves and superlensing in general photonic crystals and presented specific designs of superlenses based on AANR in photonic crystals as well as a comprehensive numerical study of their subwavelength imaging properties in 2D. Special emphasis is given to the focusing resolution and image patterns of these devices, and our studies demonstrate that the interplay between propagating and evanescent waves can lead to various image behaviors not possible with conventional lenses in geometric optics. We hope that this work should clarify the underlying physics of near-field imaging and stimulate interests of experimental studies of superlensing.

ACKNOWLEDGMENT

*Electronic address: chiyan@mit.edu
[1] V.G. Veselago, Sov. Phys. Usp. **10**, 509 (1968).
[2] J.B. Pendry, A.J. Holden, W.J. Stewart, and I. Youngs, Phys. Rev. Lett. **76**, 4773 (1996).
[3] H. Kosaka, T. Kawashima, A. Tomita, M. Notomi, T. Tamamura, T. Sato, and S. Kawakami, Phys. Rev. B **58**, 10 096 (1998).
[4] J.B. Pendry, A.J. Holden, D.J. Robbins, and W.J. Stewart, IEEE Trans. Microwave Theory Tech. **47**, 2075 (1999).
[5] J.B. Pendry, Phys. Rev. Lett. **85**, 3966 (2000).
[6] D.R. Smith, W.J. Padilla, D.C. Vier, S.C. Nemat-Nasser, and S. Schultz, Phys. Rev. Lett. **84**, 4184 (2000).
[7] D.R. Smith and N. Kroll, Phys. Rev. Lett. **85**, 2933 (2000).
[8] M. Notomi, Phys. Rev. B **62**, 10 696 (2000).
[9] R.A. Shelby, D.R. Smith, and S. Schultz, Science **292**, 77 (2001).
[10] R.A. Shelby, D.R. Smith, S.C. Nemat-Nasser, and S. Schultz, Appl. Phys. Lett. **78**, 489 (2001).
[11] R.W. Ziolkowski and E. Heyman, Phys. Rev. E **64**, 056625 (2001).
[12] C. Luo, S.G. Johnson, J.D. Joannopoulos, and J.B. Pendry, Phys. Rev. B **65**, 201104(R) (2002).
[13] J.T. Shen and P.M. Platzman, Appl. Phys. Lett. **80**, 3286 (2002).
[14] M. Bayindir, K. Aydin, E. Ozbay, P. Markos, and C.M. Soukoulis, Appl. Phys. Lett. **81**, 120 (2002).
[15] C. Luo, S.G. Johnson, and J.D. Joannopoulos, Appl. Phys. Lett. **81**, 2352 (2002).
[16] R. Marques, J. Martel, F. Mesa, and F. Medina, Phys. Rev. Lett. **89**, 183901 (2002).
[17] R.M. Walser, A.P. Valanju, and P.M. Valanju, Phys. Rev. Lett. **87**, 119701 (2001).
[18] G.W. 't Hooft, Phys. Rev. Lett. **87**, 249701 (2001).
[19] J. Pendry, Phys. Rev. Lett. **87**, 249702 (2001).
[20] J.M. Williams, Phys. Rev. Lett. **87**, 249703 (2001).
[21] J. Pendry, Phys. Rev. Lett. **87**, 249704 (2001).
[22] A. Lakhtakia, Int. J. Infrared Millim. Waves **23**, 339 (2002).
[23] P.M. Valanju, R.M. Walser, and A.P. Valanju, Phys. Rev. Lett. **88**, 187401 (2002).
[24] N. Garcia and M. Nieto-Vesperinas, Phys. Rev. Lett. **88**, 207403 (2002).
[25] N. Garcia and M. Nieto-Vesperinas, Opt. Lett. **27**, 885 (2002).
[26] A.L. Pokrovsky and A.L. Efros, Phys. Rev. Lett. **89**, 093901 (2002).
[27] F.D.M. Haldane, cond-mat/0206420, Phys. Rev. B (to be published).
[28] D.R. Smith, D. Schurig, and J.B. Pendry, Appl. Phys. Lett. **81**, 2713 (2002).
[29] J. Pacheco, T.M. Grzegorczyk, B.-I. Wu, Y. Zhang, and J.A. Kong, Phys. Rev. Lett. **89**, 257401 (2002).
[30] J. D. Joannopoulos, R. D. Meade, and J. N. Winn, *Photonic Crystals: Molding the Flow of Light* (Princeton University Press, Princeton, 1995).

[31] U. Fano, Phys. Rev. **124**, 1866 (1961).

[32] S. Peng and G.M. Morris, J. Opt. Soc. Am. A **13**, 993 (1996).

[33] V.N. Astratov, I.S. Culshaw, R.M. Stevenson, D.M. Whittaker, M.S. Skolnick, T.F. Krauss, and R.M.D.L. Rue, J. Lightwave Technol. **17**, 2050 (1999).

[34] P. Paddon and J.F. Young, Phys. Rev. B **61**, 2090 (2000).

[35] T. Ochiai and K. Sakoda, Phys. Rev. B **63**, 125107 (2001).

[36] S. Fan and J.D. Joannopoulos, Phys. Rev. B **65**, 235112 (2002).

[37] T.W. Ebbesen, H.J. Lezec, H.F. Ghaemi, T. Thio, and P.A. Wolff, Nature (London) **391**, 667 (1998).

[38] J.A. Porto, F.J. Garcia-Vidal, and J.B. Pendry, Phys. Rev. Lett. **83**, 2845 (1999).

[39] L. Martin-Moreno, F.J. Garcia-Vidal, H.J. Lezec, K.M. Pellerin, T. Thio, J.B. Pendry, and T.W. Ebbesen, Phys. Rev. Lett. **86**, 1114 (2001).

[40] In some occasions, due to reasons of modal symmetry, they can also appear in discrete locations above the light line (Ref. 34).

[41] The nonzero slope of Eq. (8) at the surface Brillouin zone edge is usually negligible.

[42] H. A. Atwater (private communication).

[43] V. Kuzmiak, A.A. Maradudin, and F. Pincemin, Phys. Rev. B **50**, 16 835 (1994).

[44] T. Ito and K. Sakoda, Phys. Rev. B **64**, 045117 (2001).

[45] S.G. Johnson and J.D. Joannopoulos, Opt. Express **8**, 173 (2001).

[46] D.M. Whittaker and I.S. Culshaw, Phys. Rev. B **60**, 2610 (1999).

[47] The transmission near exact resonances in an infinite structure requires a much higher computational resolution in principle.

[48] S.G. Johnson, S. Fan, P.R. Villeneuve, J.D. Joannopoulos, and L.A. Kolodziejski, Phys. Rev. B **60**, 5751 (1999).

[49] R. Ruppin, Phys. Lett. A **277**, 61 (2000).

[50] R. Ruppin, J. Phys.: Condens. Matter **13**, 1811 (2001).